**EUROPEAN ORGANISATION FOR NUCLEAR RESEARCH**
**CERN – A&B DEPARTMENT**

**AB-Note-2008-036 ABP**

# Updated layout of the LINAC4 transfer line to the PS Booster (Green Field Option)

G. Bellodi, M.Eshraqi, J.B.Lallement, A. M. Lombardi

## Abstract

At the time of defining the site of Linac4 and its integration in the complex of existing infrastructure at CERN (together with the plans for a future Superconducting Proton Linac), a series of radiation protection issues emerged that have since prompted a revision of the Linac4 to PSB transfer line layout, as was described in the document AB-Note-2007-037.

For radiological safety reasons the distance between the planned SPL tunnel and the basement of building 513 had to be increased, and this led to the decision to lower the Linac4 machine by 2.5m. A vertical ramp was consequently introduced in the transfer line to raise the beam at the same level of LINAC2/PSB for connection to the existing transfer line.

A series of error study runs has been carried out on the modified layout to have an estimate of the losses induced by quadrupole alignment and field errors. The two worst cases of each error family have been used as case studies to test the efficiency of possible steering strategies in minimizing beam losses and machine activation. The new layout and beam dynamics issues plus the results of the error and steering studies are discussed in this note.

*Geneva, Switzerland*
*July 2008*

## Introduction

At the time of defining the implementation of Linac4 and its integration in the complex of the existing and future infrastructure at CERN, some radiological safety concerns resulted in the decision to lower the depth of the machine tunnel by 2.5m in order to reduce the incidence onto the basement of building 513 of the radiation emitted from the SPL (planned as a continuation of LINAC4 and aligned to it on its surface projection, but on a 1.7% downward slope). A vertical ramp had consequently to be introduced in the transfer line branching out of LINAC4 towards the PS Booster, in order to raise the beam to the same level of LINAC2 and the PSB before connecting to the existing transfer line at the position of the BHZ20 dipole magnet (see document AB-Note-2007-037 for details of the layout).

## Layout

The structure of the transfer line has hence been modified with the addition of a vertical 'step' in the straight section between the debuncher cavity and the LT.BHZ20 dipole (see Fig.1) and a few extra quadrupoles for beam matching at its entrance and exit.

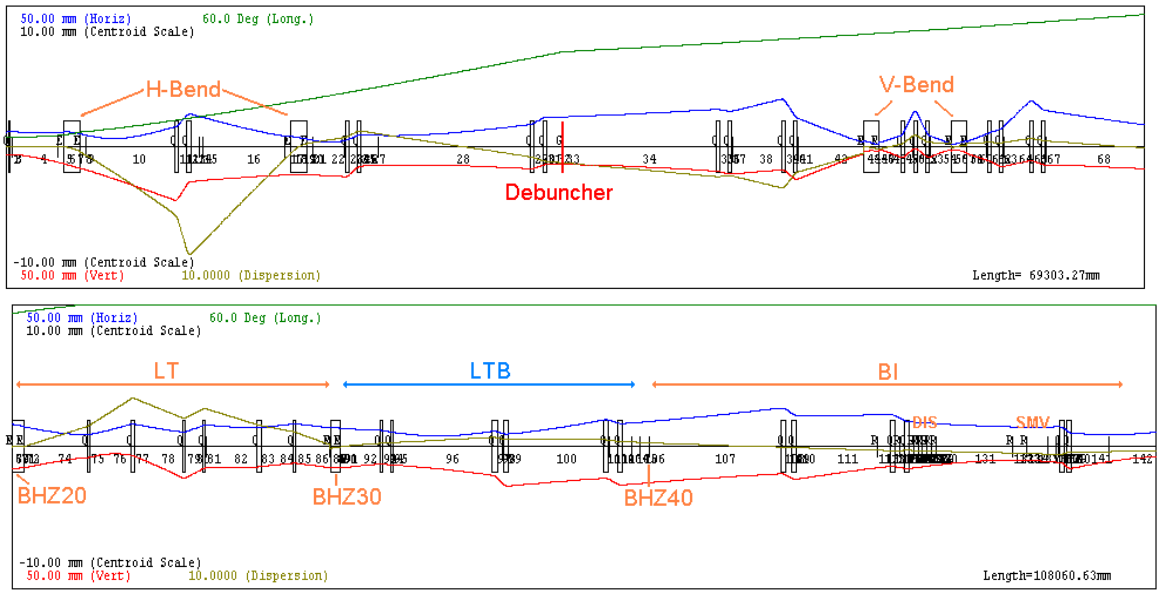


**Fig. 1 Sketch of the transfer line showing magnet positions, beam envelopes (in red and blue), longitudinal phase spread (green) and zero current dispersion (ochre).**

The beam is deflected on an upward ramp and brought back to level by means of two vertical dipoles of 1m in length and separated by approximately 5m (giving a slope of roughly 50%), with a bending angle of ±27.85 deg for an applied field of 1T. A quadrupole triplet is inserted between the two dipoles to make this part of the transfer line achromatic (see Fig. 2 and 3 for schematic views).

The quadrupole doublets downstream of the debuncher cavity have been repositioned for a better beam matching at the entrance and exit of the ramp and an extra doublet has been introduced before LT.BHZ20.

Also, two of the six quadrupoles that were coupled in pairs on the same power supply in this section (pre-step) have been moved onto separate supplies in order to build more flexibility into the beam dynamics design.

Other modifications only recently introduced to achieve a leaner design concern the first bend at the exit of LINAC4: here the length of the two horizontal dipoles has been reduced to make them similar in dimensions to the two vertical dipoles and group all four into a single family thus reducing the costs of drawing and production. Transverse focusing in this section was slightly changed with the suppression of one quadrupole found to be redundant. Finally, in the area where the LINAC4 tunnel intersects the LINAC2 building, additional radiological concerns have prompted the repositioning of two quadrupoles upstream outside the walls of the building, in order to reduce the amount of extra shielding needed in the area to something localized only around the beam pipe in the absence of any magnets.
The inventory of all the transfer line elements in the section to be newly built up to LT.BHZ20 is thus summarized in Table 1 (beam diagnostics excluded).

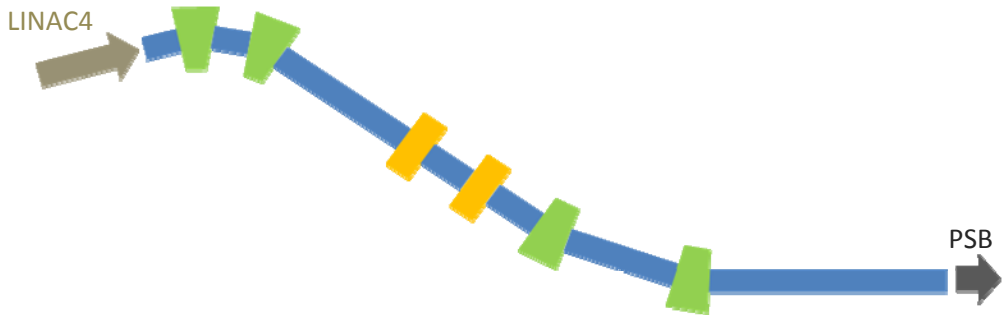


**Fig. 2. Schematic top view of the transfer line from LINAC4 to PSB (not to scale). Green blocks indicate horizontal bends, while the yellow elements stand for vertical dipoles.**

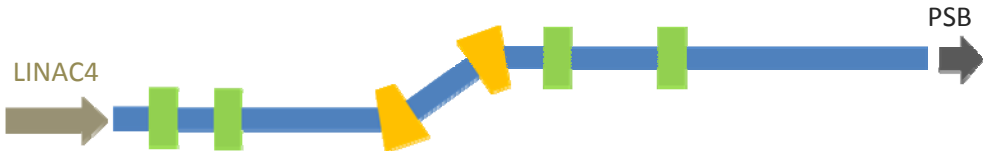


**Fig. 3. Schematic side view along the beam direction (not to scale).**

| Bending magnets | | | Quadrupoles | | Debuncher cavity | |
|---|---|---|---|---|---|---|
| | H | V | | | | |
| Number of magnets | 2 | 2 | Number of magnets | 17 | Number of cells | 5 |
| Number of power supplies | 1 | 1 | Number of power supplies | 15 | | |
| Deflection angles (Deg) | 35 | 27.85 | Max gradient (T/m) | 15 | Applied voltage | 0.7MV |
| Effective length (m) | 1 | 1 | Aperture radius (mm) | 50 | | |
| Magnetic field (T) | 1.2 | 1 | Magnetic length (mm) | 250 | | |
| Vertex Angle (Deg) | 35 | 35 | | | | |

**Table 1 Inventory of the transfer line components up to LT.BHZ20.**

## Beam dynamics

Beam dynamics in the transfer line has been studied with multi-particle simulations using the code PATH and an input beam distribution of approximately 45k particles resulting from end-to-end tracking from the RFQ to the last PIMS cavity of the linac. Figure 4 shows the phase

space plots at the beginning of the transfer line, and Table 2 summarises the main beam specifications.

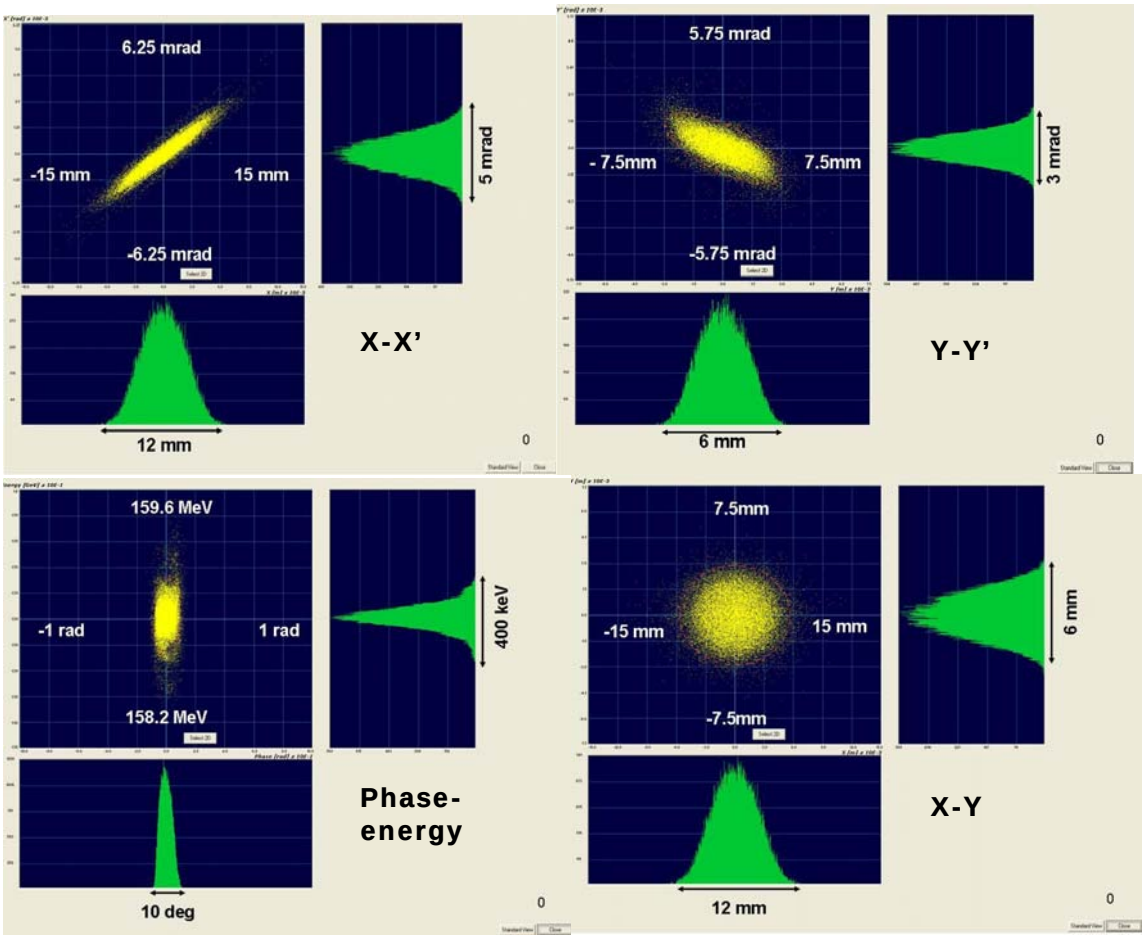


**Fig. 4 Phase space plots of the input beam distribution (from end-to-end tracking through Linac4) at the beginning of the transfer line (x-x', y-y', x-y and $\Delta E$–$\Delta\phi$ planes respectively from top left in clockwise order).**

| | $\alpha$ | $\beta$ | $\varepsilon_{RMS}$ |
|---|---|---|---|
| x | -3.40 | 10.02 m/rad | 0.345 mm mrad |
| y | 0.97 | 2.71 m/rad | 0.328 mm mrad |
| z | -0.13 | 28.06 deg/MeV | 0.178 deg MeV |
| Energy | 158.91 MeV | | |
| Microbunch current | 65 mA | | |
| Frequency | 352.2 MHz | | |
| Energy spread | 80.3 keV (RMS) | | |

**Table 2 Twiss parameters and RMS normalized emittance values for the input beam distribution.**

The introduction of a vertical step has made necessary a retuning of the transfer line, under the same guidelines that informed the design of the 'flat' version of the line, discussed in detail in AB-Note-2007-037: namely control of transverse emittance growth and dispersion function during beam transport and satisfaction of the final matching requirements at injection into the

PS Booster in the frame of the transverse and longitudinal painting schemes currently envisaged.

The initial part of the line, where the beam is deflected towards LINAC2 through a double bend has only been changed with the suppression of one quadrupole found to be redundant: the settings used for the magnets in this section are those that were found to minimize the emittance growth in a strongly space charge dominated regime. The beam is then transported through a 33m long straight section via a doublets structure; a debuncher cavity (5-cells, 1.1 m long, with an applied voltage of 0.7MV at 352MHz), located at approximately 34m from the LINAC4 exit, is used to reduce the energy spread of the beam in this section. The beam is then raised vertically by 2.5m to the level of LINAC2 via a ramp with close to 50% slope.

An achromatic solution, reached by tuning of a quadrupole triplet inserted between the two vertical dipole magnets, has been adopted for the ramp in order to minimize any dispersive effects in the vertical plane and at the same time to avoid any coupling between the two transverse planes that could arise from the horizontal and vertical dispersion crosstalk. Sizeable vertical dispersive effects would not be tolerable given the narrow acceptances needed downstream in the distributor and septum magnets for beam separation into the four separate Booster rings; similarly, any residual coupling would also have to be eliminated via the addition of skew quadrupoles. The solution here presented limits D and D' in the vertical plane to 0.01m and 1% respectively along most of the line.

The two doublet pairs immediately preceding and following the slope have been used for matching the beam at the entrance of the first vertical dipole on one side and at the exit from the second onto the next section up to LT.BHZ20 on the other. The quadrupoles that in the original design had been connected onto the same power supply have been separated in the present scheme in order to allow for more flexibility and capability of tuning in the transfer line. After the joining point with the existing LINAC2 transfer line at the location of the LT.BHZ20 dipole, the six quadrupoles between LT.BHZ20 and LT.BHZ30 have been found to be the most efficient knobs to control the horizontal dispersion along the line. Apart from aiming to match the required values of D and D' at injection in the Booster, two additional targets are closing the full current dispersion bump at the exit of LT.BHZ30 to reduce emittance growth in the horizontal plane, and at the same time reducing the height of the zero current dispersion peak between the two dipoles to keep a sufficiently large energy acceptance. The settings here adopted therefore represent a balance between these three objectives.

Finally, the six quadrupole doublets in the LTB-BI part of the line, after the LT.BHZ30 dipole, have been used for modulating the beam envelopes to match injection conditions at the Booster. Following indications from transverse painting studies (to achieve the small emittance required for the LHC beam one has to minimize mismatch at injection and therefore arrive with Twiss parameters as close as possible to the Booster closed orbit solution), the aim has been to keep the final beta functions at the injection point as small as possible.

PATH simulation results for tracking through the transfer line with an end-to-end initial beam distribution and rings-of-charge space charge modeling are shown in Figs. 5-9.

Fig.5 shows the RMS emittance evolution along the transfer line (inclusive of the combined effect of energy spread and dispersion, as is evident in the steps occurring at dipole positions). The overall growth along the 180m length amounts to approximately 20% and 44% for the horizontal and vertical planes respectively (with final normalized RMS values of 0.42 and 0.47 $\pi$ mm mrad). Applying some collimation on the initial beam distribution to eliminate some of the halo transmitted by the linac (about 3% of the beam particles), one can reduce the transverse emittance growth to 7% and 30% in the horizontal and vertical planes respectively.

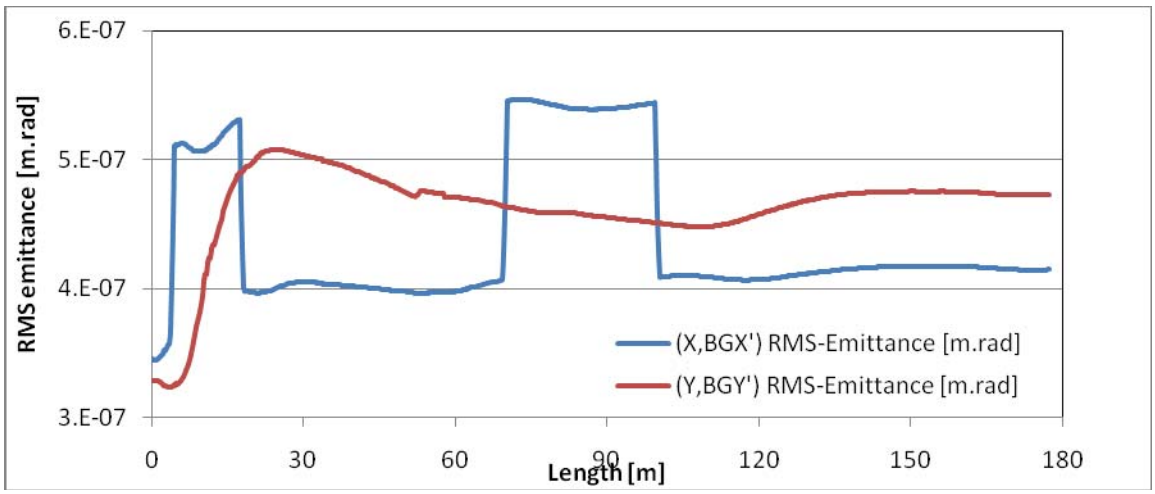


**Fig. 5. Evolution of the transverse RMS normalized emittances.**

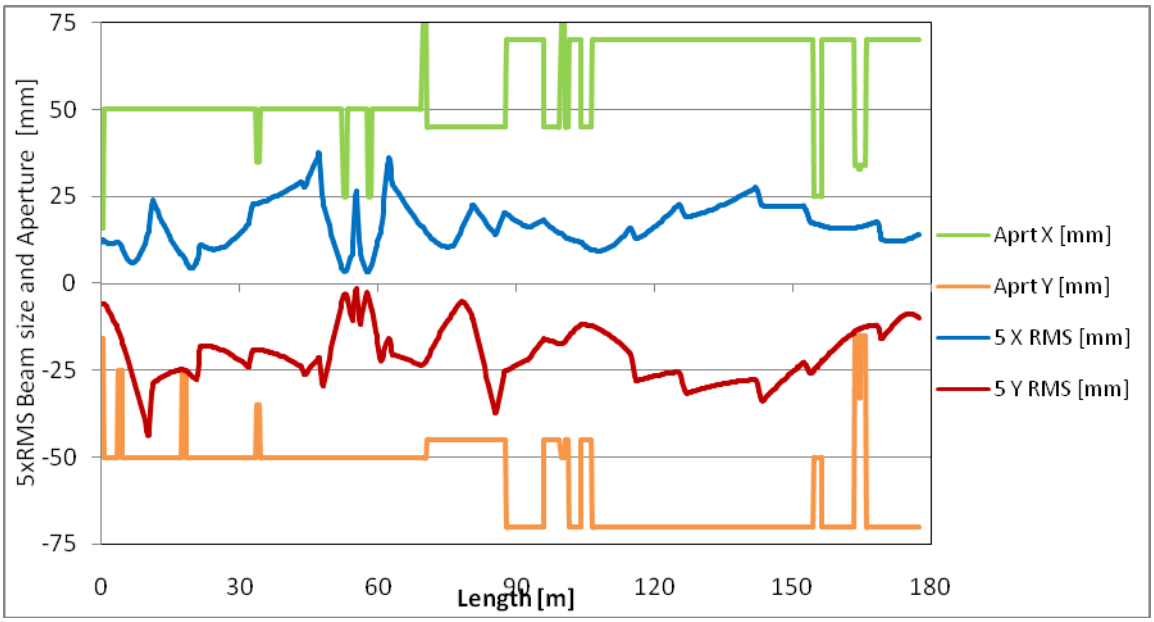


**Fig. 6. 5 × RMS transverse beam envelopes and physical aperture.**

Fig.6 shows the 5σ beam envelopes in comparison with the physical radial aperture along the transfer line. There are a few main bottlenecks: one vertically between the two initial horizontal bends, one horizontally in the dispersive area between the LT.BHZ20 and LT.BHZ30 dipoles, and one vertically located just downstream. A radial aperture of 50mm has been assumed for the length of beampipe to be newly built (apart from a restriction to 35mm at and around the debuncher cavity), whereas the existing values have been taken for the part of the transfer line after LT.BHZ20 (namely 45 and 70mm depending on the sections).

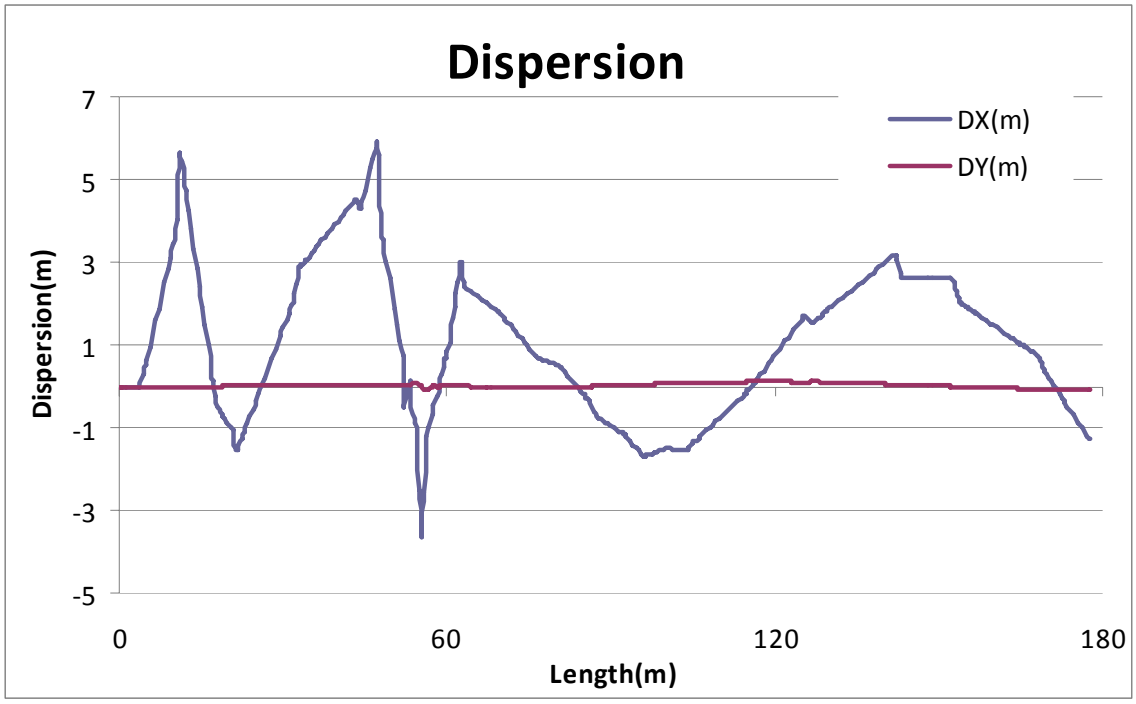


**Fig. 7. Horizontal and vertical dispersion, from the beam centroid displacement in full current case.**

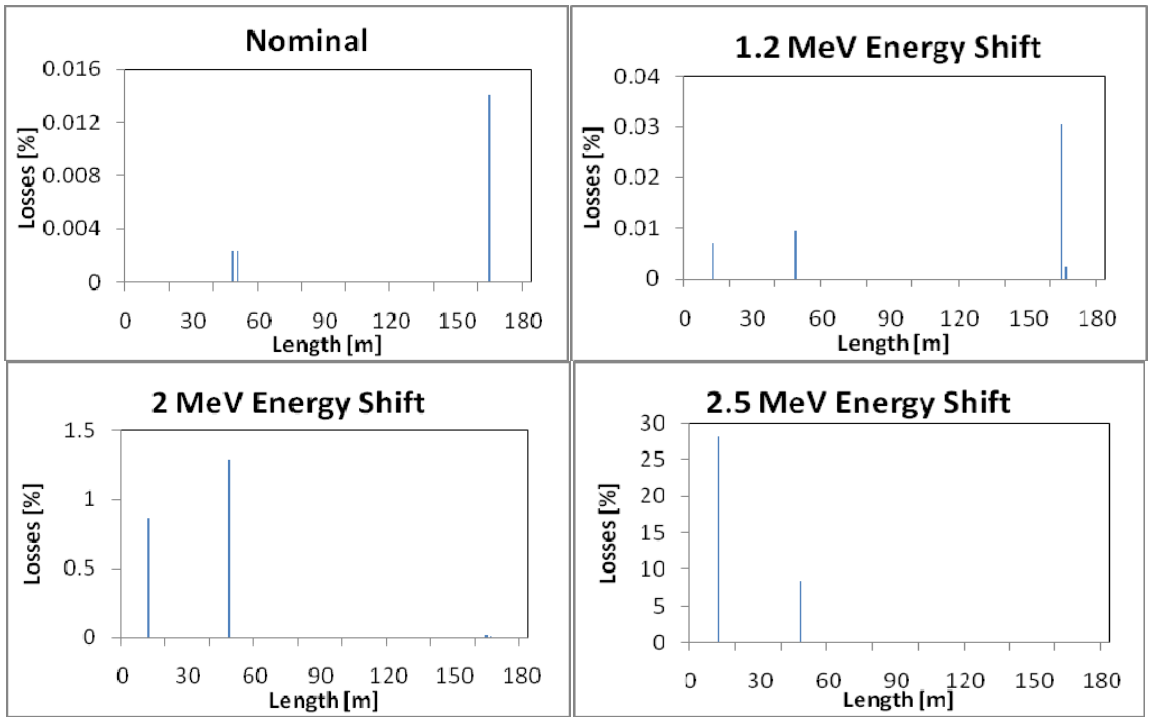


**Fig. 8. Beam losses histogram along the length of the transfer line for the nominal case (top left), with applied energy offsets: ΔE=1.2 MeV (top right), ΔE=2MeV (bottom left), and ΔE=2.5MeV (bottom right).**

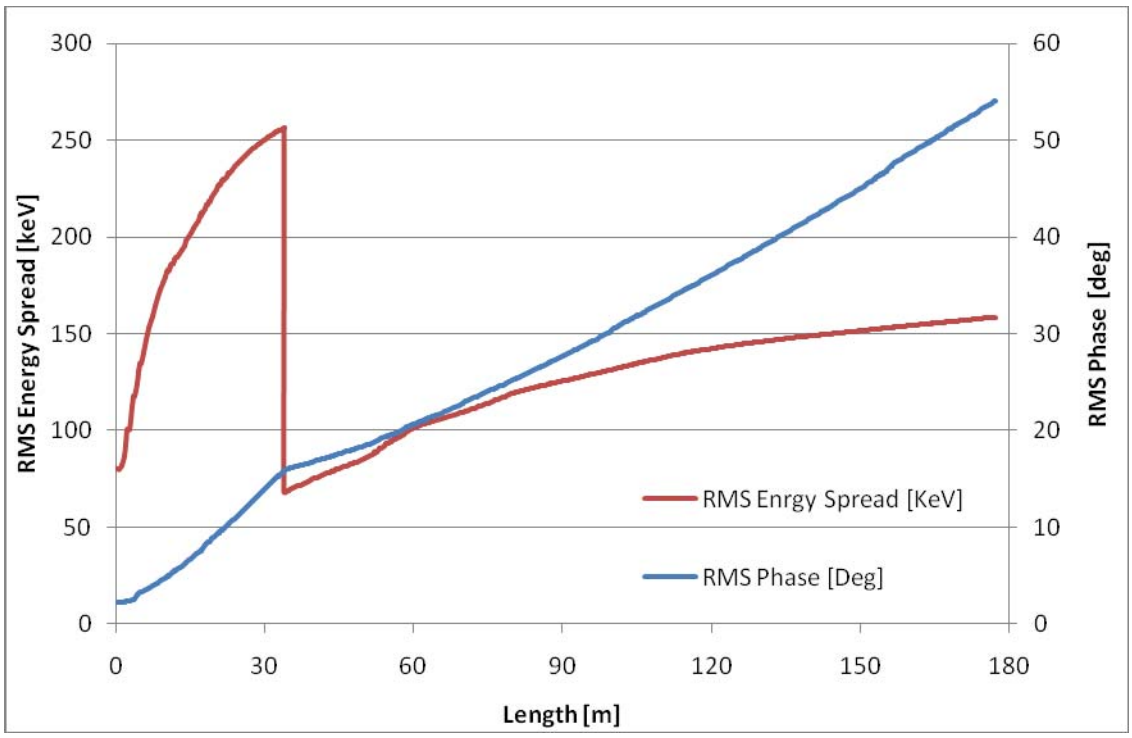


**Fig. 9. Evolution of the RMS energy spread and phase width along the transfer line.**

Fig.7 shows the horizontal and vertical dispersion along the transfer line, as given by the beam centroid displacement resulting from an initial 0.1% momentum kick. The vertical dispersion has been rematched to approximately zero at the exit of the ramp, whereas in the horizontal plane the line has been tuned to match the zero current dispersion values of the closed orbit solution in the PS Booster at the injection point ($D_x$=-1.42m and $D'_x$=0, see document AB-Note-2007-037 for a more detailed discussion on the subject). The quadrupole settings for this solution are listed in Appendix A.

The dispersion profile affects the energy acceptance of the transfer line by converting beam momentum jitter into a transverse beam position displacement, with potential risk of losses. As shown in Fig.8, total losses for the nominal case are below 0.1%; the transmission is still good (less than 0.1% losses) for an energy offset of 1.2 MeV, corresponding to the maximum excursion in the energy ramp currently envisaged for a longitudinal painting scheme at the PSB injection. However, beam losses are already significant (around 2%) for an energy offset of 2 MeV, approximately equivalent to the sum of the contributions of the longitudinal painting with three times the estimated RMS value of the energy jitter propagated down from the linac.

As for the longitudinal plane, Fig.9 shows the evolution of the beam RMS energy spread and phase width under the effect of the space charge forces and the applied external 0.7MV cavity voltage. The values reached at injection in the Booster are 158keV and 54 deg respectively.

| | $\alpha$ | $\beta$ | $\varepsilon_{RMS}$ |
|---|---|---|---|
| x | -0.634 | 11.73 m/rad | 0.415 mm mrad |
| y | -0.5 | 5.03 m/rad | 0.473 mm mrad |
| Phase width | 54 deg (RMS) | | |
| Energy spread | 158 keV (RMS) | | |
| $D_x$ (m) | -1.07 | | |
| $D'_x$ (rad) | -0.16 | | |
| $D_y$ (m) | 0.05 | | |
| $D'_y$(rad) | 0.01 | | |

**Table 3 Parameters of the output beam distribution.**

Fig. 10 shows the phase space plots for the end-to-end output beam distribution at the point of injection in the PS Booster (stripper foil position), and Table 3 summarises the main beam parameters at this location (Twiss parameters and emittances are calculated with PATH multiparticle simulation, while dispersion values are calculated with Trace3D for the beam center).

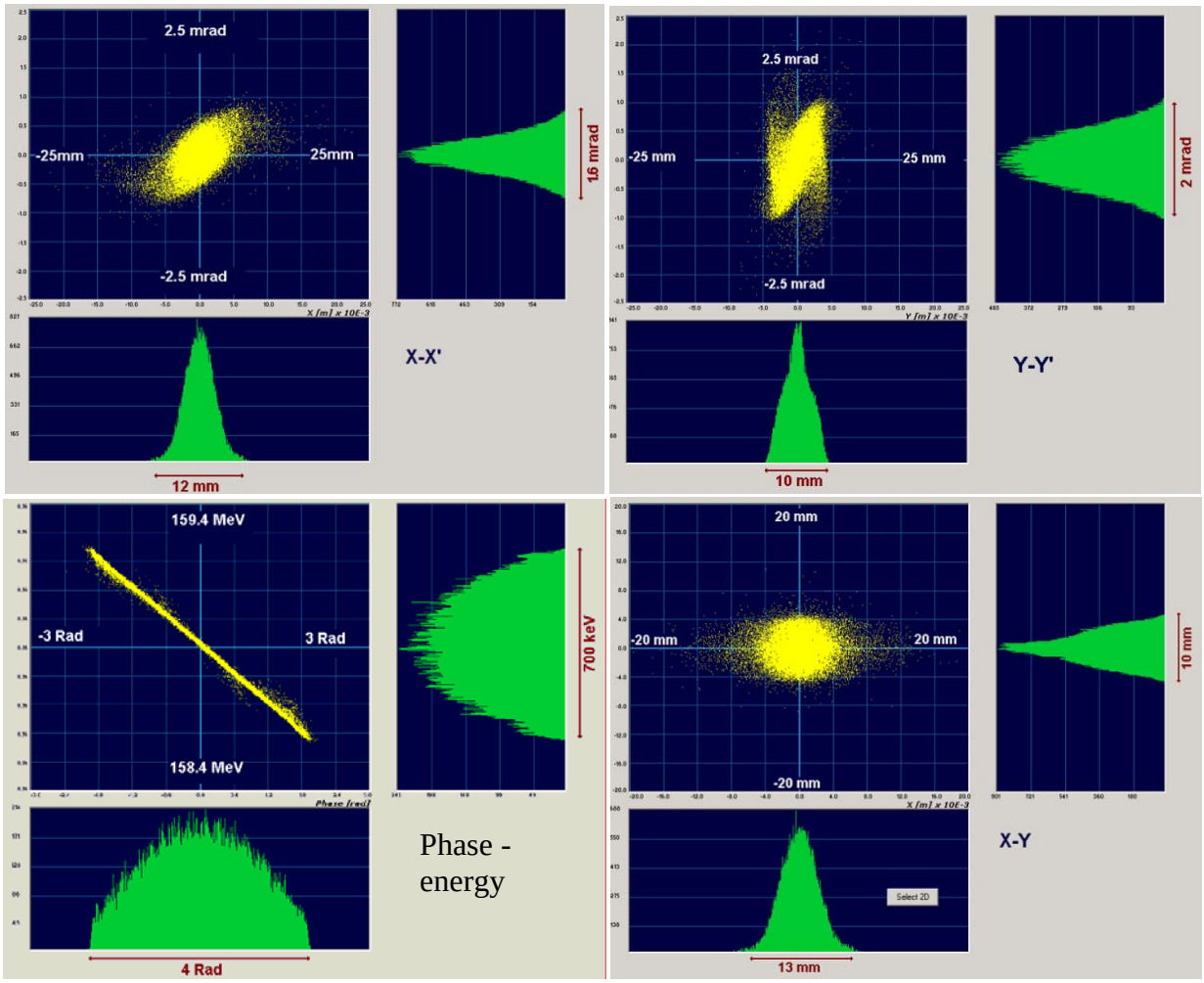


**Fig. 10. Phase space plots of the end-to-end output beam distribution at the end of the transfer line (showing respectively the x-x', y-y', x-y and $\Delta E$–$\Delta\phi$ planes from the top left picture in clockwise order).**

## Error Study

A campaign of error study has been carried out to assess the risk of beam losses and consequent machine activation. To avoid statistical limitations, 1000 runs were performed for each set of errors, using an input beam distribution of approx. 45k particles. The errors applied fall within two categories: initial beam errors and quadrupole errors. *Initial beam errors* are given by displacements of the beam center in both the horizontal (X-X') and vertical (Y-Y') planes. *Quadrupole errors* include *gradient errors* (deviation of the quadrupolar field from the nominal value), *transverse misalignments* (offset between the position of the beam trajectory and the quadrupole magnetic center in the two transverse planes), and *angle errors* (3 angles that express the rotation of the quadrupole around the design beam trajectory). The error distribution can be either uniform or Gaussian with a cut at *3× sigma*.

## Figures of merit and constraints.

Quadrupole errors (position, gradient and rotation) can induce beam losses, emittance growth, trajectory errors, correlation between vertical and horizontal planes, and also affect dispersion. Beam loss is the most important quantity to control, since it is the cause of potential irradiation of the machine, hence the need of accurate predictions to be able to dimension correctly the necessary amount of shielding. Next priority is the emittance increase, that should be controlled to maintain the quality of the beam which is going to be injected into the PS booster. Finally, beam center excursion should be limited to reduce the number and strength of the steerers and also to avoid nonlinear effects that may occur when the beam moves into the "bad field" area of the magnetic elements at higher radius (emittance growth in quadrupoles increases with the second power of the quadrupole misalignment value). Dispersion all along the line should be kept lower than 5m to avoid significant transverse offsets of off-momentum particles and consequent risk of losses ; also correlation between planes must be controlled.

A compromise should be found which, while keeping all aforementioned quantities within certain acceptable values, does not increase the cost of machining and alignment beyond a reasonable budget. In our case, the criteria we have followed to establish the scale of quadrupole errors that can be tolerated are listed below:

a) Maximum average losses of 1 W/m which is dictated by shielding requirements.

$$Power\ loss\ (W) = \frac{\#\ of\ lost\ particles \times Current\ (A) \times Energy\ (MeV) \times Duty\ cycle}{Number\ of\ particles\ in\ Simulation}$$

b) Maximum localized losses should not exceed 1W after steering. This allows hands-on maintenance.

c) Emittance growth of less than 15% with respect to the nominal case (defined by the emittance budget in the PS Booster).

d) Correlation between vertical and horizontal plane, $\alpha_{xy} < 0.1$.

e) Dispersion at injection point in the PS booster should be within 0.4m of the target value.

## Purposes and Procedure

Two are the main goals to be achieved with this study: the first is to define the tolerances on quadrupole gradients, misalignments and rotations, so that the effect of these errors is within the constraints defined in the previous paragraph. The second aim is to establish the necessary number of corrective elements (steering magnets) and their corresponding diagnostics (beam profile monitors) and find their appropriate location.

## Error study results and steering

The errors applied in the study here presented are:

an initial beam jitter of 0.3 mm in the transverse position and 1 mrad in divergence in both the vertical and horizontal planes, following a Gaussian distribution cut at 3 × sigma;

quadrupole errors of 0.5% in gradient, 0.2 deg in rotation around the beam axis and 0.4/0.5 mm misalignment, all following a uniform distribution.

These have been studied separately or combined (see Table 4 for results).

| alignment | Beam Error | $\Delta\varepsilon_x$ %RMS | $\Delta\varepsilon_y$ %RMS | Trans % | $\alpha_{xy}$ | $\alpha_{xy'}$ | $\alpha_{x'y}$ | $\alpha_{x'y'}$ | Dx m | D'x | Dy m | D'y |
|---|---|---|---|---|---|---|---|---|---|---|---|---|
| 0.4 mm | × | 2.25±0.35 | -1.41±0.02 | 89.0±23 | -2.17E-3 | -1.47E-2 | 6.75E-2 | -7.77E-2 | -1.6±5.2 | 0.01 | -1.3±9.25 | 0.05 |
| 0.4 mm | √ | 9.76±2.17 | 3.37±0.68 | 72.9±34 | 5.93E-3 | -1.08E-2 | 6.63E-2 | -7.0E-2 | -1.7±7.5 | -0.05 | -0.6±9.35 | 0.06 |
| 0.5 mm | × | 8.5±1.87 | 6.43±1.57 | 72.3±37 | -1.09E-2 | -2.36E-2 | 6.30E-2 | 2.22E-2 | -1.2±6.5 | 0.02 | -0.09±10 | 0.02 |
| 0.5 mm | √ | 14.6±4.32 | 9.17±2.76 | 60.9±39 | -9.22E-3 | -1.38E-2 | 5.35E-2 | -5.8E-2 | -1.5±7.7 | 0.01 | -0.8±10 | 0.04 |

**Table 4. Results of the error study before steering (showing emittance variation, final transmission, correlation between planes and dispersion values at injection in the Booster). In all cases a rotation error of 0.2 deg and gradient error of 0.5% are applied on the magnets.**

Emittance growth and correlation between vertical and horizontal planes are within the stated limits; errors have quite a significant effect on the dispersion values at injection in the PS Booster. A further study has been carried out to try to recover transmission by steering the beam trajectory with the aid of correction elements, kickers and screens at an appropriate location and strength.

| alignment | Beam Error | $\Delta\varepsilon_x$ %RMS | $\Delta\varepsilon_y$ %RMS | Transmission % |
|---|---|---|---|---|
| **0.4 mm** | × | -6.04 | 11.30 | 99.96 |
| **0.4 mm** | × | 9.62 | -1.30 | 99.94 |
| **0.4 mm** | √ | 5.37 | 15.00 | 99.96 |
| **0.4 mm** | √ | 7.61 | 10.00 | 99.95 |
| **0.5 mm** | × | 7.38 | 13.91 | 99.94 |
| **0.5 mm** | × | 3.13 | 7.39 | 99.92 |
| **0.5 mm** | √ | -5.59 | 9.78 | 99.94 |
| **0.5 mm** | √ | 8.50 | 5.43 | 99.97 |

**Table 5. Results of the steering study for the two worst cases for beam losses when applying a 0.4/0.5 mm misalignment errors on the transfer line quadrupoles, with and without initial beam jitter . Columns show emittance growth and final transmission results.**

## Steering

In the scheme devised for this study, two steerers, one in the vertical plane and one in the horizontal plane, are assigned to each doublet in the new section of the line, starting from the end of LINAC4 up to BHZ20. Downstream of BHZ20 we have assumed the same number and position of steerers and screens which are presently in the LINAC2 transfer line.

To study the efficiency of the chosen scheme, the two worst cases for losses all over the transfer line have been selected, and we looked for values of the steerers' strength that would minimize the beam center excursion at the location of the given diagnostics. If no converging solution is found, the position of the steerers (or of the diagnostics) is changed and the process repeated. A maximum of 4mT.m has been taken as maximum value for the kicks.

Four different cases have been studied, for a 0.4 / 0.5 mm misalignment error with /without initial beam jitter respectively. In all of them a rotation error of 0.2 degrees and a gradient error of 0.5% have been applied. Transmission results before and after steering for the 4 individual cases are presented in Table 5. All remnant losses after steering are shown in Fig 11.

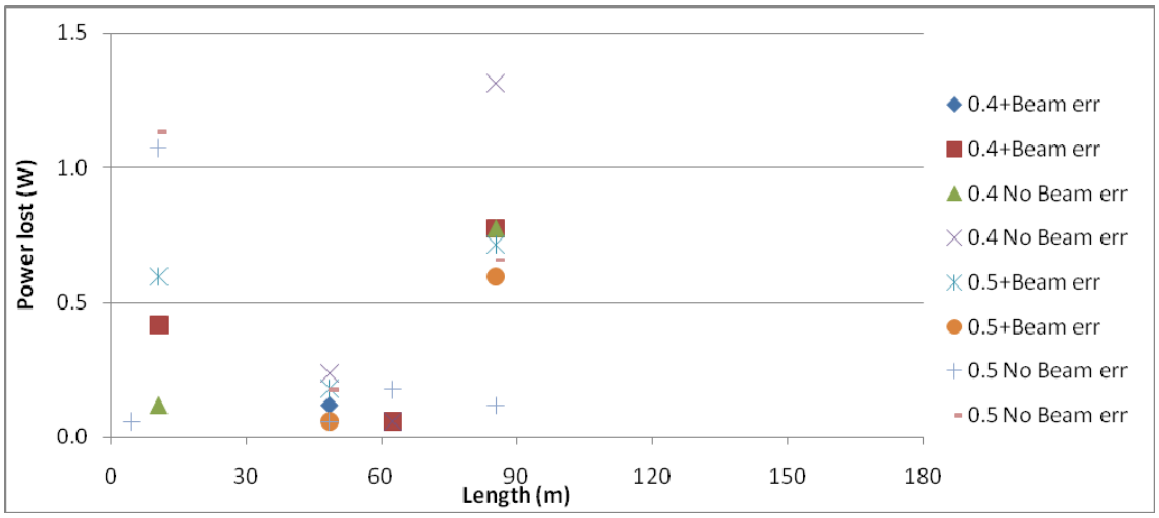


**Fig. 11. Loss map along the transfer line for the two worst cases for losses after steering (beam power is calculated for the nominal Linac4 duty cycle of 0.08%).**

## Conclusions

The note describes an updated layout of the Linac4 to PSB transfer line, prompted by a recent decision to lower the Linac4 machine tunnel by 2.5m in order to reduce the radiological impact of the planned SPL on building 513 at CERN. This has made necessary to introduce a vertical ramp in the transfer line scheme, as described in AB-Note-2007-037, in order to raise the beam at the exit of Linac4 to the same level as the PSB before injection.

In the solution here presented, low loss beam transport along the 180m length of the transfer line has been achieved under controlled transverse emittance growth conditions. Matching conditions at arrival in the PS Booster have been satisfied within the specified tolerances. Vertical dispersive effects, potentially associated to the introduction of the vertical ramp, have been minimized as is the coupling between transverse planes due to dispersion crosstalk. Certain flexibility has been built in the line in order to leave a tunability margin for different matching requirements that could be specified in the future as injection studies progress.

A campaign of error studies has also been carried out to identify potential loss spots and help devise an adequate beam steering strategy.

## Appendix A

**Table 6. Details of the transfer line elements and settings for a final beam case as specified in Table 3 (match to PSB closed orbit parameters at injection). From left to right: the longitudinal coordinate of the center (m), the magnetic length (mm), quadrupole gradients (T/m), dipole bending angles (deg), debuncher voltages (MV), and aperture values (numbers with an R indicate a circular aperture).**

| Element | $S_{center}$ (m) | Magnetic length (mm) | Gradient (T/m) | Angle (deg) | Voltage (MV) | Aperture | |
|---|---|---|---|---|---|---|---|
| | | | | | | Hor. (mm) | Ver. (mm) |
| Dipole1 | 4.25 | 1000 | | 35 | | 100 | 50 |
| Quad1 | 10.49 | 250 | 4.55 | | | R 50 | |
| Quad2 | 11.23 | 250 | -5.08 | | | R 50 | |
| Dipole2 | 18.07 | 1000 | | 35 | | 100 | 50 |
| Quad4 | 20.85 | 250 | 4 | | | R 50 | |
| Quad5 | 21.6 | 250 | -5.25 | | | R 50 | |
| Quad6 | 32.15 | 250 | 2.4 | | | R 50 | |
| Quad7 | 32.9 | 250 | -2.4 | | | R 50 | |
| Debuncher1 | 33.9 | 1150 | | | 0.7 | R 35 | |
| Quad8 | 43.45 | 250 | -0.84 | | | R 50 | |
| Quad9 | 44.2 | 250 | 1.5 | | | R 50 | |
| Quad10 | 47.45 | 250 | -4.7 | | | R 50 | |
| Quad11 | 48.2 | 250 | 4.7 | | | R 50 | |
| Vert Dipole 1 | 53.17 | 1000 | | 27.85 | | 50 | 100 |
| Quad12 | 54.7 | 250 | 15.455 | | | R 50 | |
| Quad13 | 55.47 | 250 | -14.5 | | | R 50 | |
| Quad14 | 56.24 | 250 | 15.455 | | | R 50 | |
| Vert Dipole 2 | 58.51 | 1000 | | -27.85 | | 50 | 100 |
| Quad15 | 59.98 | 250 | -0.95 | | | R 50 | |
| Quad16 | 60.73 | 250 | 4.4633 | | | R 50 | |
| Quad17 | 62.51 | 250 | -5 | | | R 50 | |
| Quad18 | 63.29 | 250 | 2.38 | | | R 50 | |
| LT.BHZ20 | 70.38 | 1094 | | -24.1 | | 150 | 100 |
| LT.QFN50 | 76.56 | 255 | 1.2 | | | R 45 | |
| LT.QDN55 | 80.79 | 255 | -1.67 | | | R 45 | |
| LT.QFN60 | 85.66 | 255 | 2.45 | | | R 45 | |
| LT.QDN65 | 87.58 | 255 | -1.65 | | | R 45 | |
| LT.QFW70 | 92.82 | 467 | 0.25 | | | R 70 | |
| LT.QDN75 | 96.1 | 255 | -0.9 | | | R 45 | |
| LT.BHZ30 | 100.34 | 1006 | | -22 | | 150 | 100 |
| LTB.QFN10 | 104.28 | 255 | -0.8 | | | R 45 | |
| LTB.QDN20 | 105.27 | 255 | 0.2 | | | R 45 | |
| LTB.QFW30 | 115.13 | 461 | -1.3 | | | R 70 | |
| LTB.QDW40 | 116.13 | 461 | 1.25 | | | R 70 | |
| LTB.QFW50 | 125.68 | 461 | -0.8 | | | R 70 | |
| LTB.QDW60 | 126.98 | 461 | 0.7 | | | R 70 | |
| BI.Q10 | 142.42 | 462 | -0.94 | | | R 70 | |
| BI.Q20 | 143.42 | 462 | 0.95 | | | R 70 | |
| BI.Q30 | 152.74 | 462 | -0.7 | | | R 70 | |
| BI.Q40 | 154.04 | 462 | 0.69 | | | R 70 | |
| BI.Q50 | 168.69 | 466 | -1.75 | | | R 70 | |
| BI.Q60 | 169.44 | 466 | 1.95 | | | R 70 | |
| end | 177.35 | | | | | | |